

This material may be downloaded for personal use only. Any other use requires prior permission of the American Society of Civil Engineers.  
This material may be found at <https://ascelibrary.org/doi/10.1061/JBENF2.BEENG-5893>.

Please cite this paper as:

Cai Q, Chen Z and Zhu S (2022) Experimental study of influence line-based damage localization for long-span cable-suspension bridges. *ASCE Journal of Bridge Engineering*. 28(3): 04022151. <https://doi.org/10.1061/JBENF2.BEENG-5893>

# Experimental Study of Influence Line-based Damage Localization for Long-span Cable-suspension Bridges

Qinlin CAI<sup>1</sup>, Zhiwei CHEN<sup>2</sup>, Songye ZHU, M.ASCE<sup>3,\*</sup>

1. Department of Civil and Environmental Engineering, The Hong Kong Polytechnic University, Hong Kong, China. Email: [qinlin.cai@polyu.edu.hk](mailto:qinlin.cai@polyu.edu.hk)

2. Department of Civil Engineering, Xiamen University, Xiamen, China. Email: [cezhiwei@xmu.edu.cn](mailto:cezhiwei@xmu.edu.cn)

3. Department of Civil and Environmental Engineering, The Hong Kong Polytechnic University, Hong Kong, China. Email: [songye.zhu@polyu.edu.hk](mailto:songye.zhu@polyu.edu.hk)

\* Corresponding author: Prof. Songye ZHU, Email: [songye.zhu@polyu.edu.hk](mailto:songye.zhu@polyu.edu.hk)

## Abstract

Influence lines (ILs)-based damage indices for long-span bridges were investigated in this study. Their effectiveness was experimentally validated for the first time through the scaled physical model of the Tsing Ma Bridge (TMB). First, the IL mechanism for damage detection and its corresponding damage indices are briefly introduced. Subsequently, the scaled TMB model instrumented with different types of sensors, including displacement sensors, strain gauges, and accelerometers, was introduced. The IL characteristics of different bridge components were compared. Two different damage cases with single and double damage locations at the bottom chord were tested. In the single-damage case, different ILs extracted from the nearby components were used for damage identification. These ILs could successfully locate damage visually. The strain IL (SIL) was more sensitive to local damage than deflection IL, but its detection performance degrades rapidly with the increasing distance between sensor and force locations. In the double-damage case, the SIL extracted from a single sensor cannot identify both damages because of the limited detectable range of each SIL; using multiple sensor information was necessary. For comparison, the modal parameters were also employed for damage detection. These experimental results validated the merits of the IL-based methods proposed for long-span bridges, indicating that IL-based damage indices are good indicators of local damage detection in long-span bridges. This finding contributes to the development of real-time techniques for damage localization in long-span bridges equipped with a structural health monitoring system.

**Keywords:** influence line; damage detection; long-span bridge; structural health monitoring

## Introduction

### *Vibration-based Damage Indices*

Once built, bridges suffer from continuous deterioration and damage accumulation caused by the long-term effects of traffic loads and harsh environmental conditions. Bridge health monitoring systems aiming to monitor bridge operation conditions and guarantee bridge safety and functionality during the service life of bridges have been installed on many bridges, particularly long-span bridges, such as Tsing Ma Bridge (TMB) (Wong et al. 2000), Jindo Bridge (Jang et al. 2010), and Sutong Bridge (Zhang et al. 2022). Bridge health monitoring systems employ different types of sensors and collect a great deal of data and information. Different vibration-based techniques, often classified into frequency- and time-domain categories, have been actively proposed to detect the anomalies of bridges. The well-known family of vibration-based frequency domain approaches is based on the change in structural dynamic characteristics and their derivatives. For example, Xu and Wu (2007) and Xu et al. (2011) proposed using acceleration and strain responses-based energy strategies to detect damages in long-span bridges. Ni et al. (2008) employed the relative flexibility change as a damage index to detect damages in the cable-stayed Ting Kau Bridge, where various structural components were simulated to be damaged. Wickramasinghe et al. (2016) conducted a laboratory experiment on a scaled suspension bridge model to validate their proposed mode shape-based damage index. Thus far, other dynamic characteristics proposed for damage detection include, but are not limited to, natural frequencies (Cawley and Adams 1979), frequency response functions (Liu et al. 2009), mode shapes (Pandey and Biswas 1991), and so on. These dynamic characteristics have been employed for model updating (Sharry et al. 2022; Ren et al. 2022; Briseghella et al. 2022) and performance evaluation (Wang et al. 2022b) of bridge structures. However, after a series of field experiments, it is noted that these structural dynamic characteristics are typically insensitive to local structural damage or have a low resistance to the operating environmental factors (e.g., temperature) (Chen et al. 2015; 2018). Moreover, mode shape-oriented approaches typically require measurement at sufficient locations to configure accurate spatial distribution (He and Zhu 2016). These constraints limit real-world applications of these approaches.

The sensors required in time-domain methods are fewer than those required in the frequency-domain methods (Li and Zhao 2006). In particular, moving loads, which resemble vehicles running on a bridge, can provide a signal with large amplitudes and high signal-to-noise ratios when they pass through the sensor locations (Link and Weiland 2009). Such moving load-based methods have attracted growing attention in recent years (Lu and Law 2007; He and Zhu 2016; He et al. 2017). In addition, other non-parameter-based methods have also been

reported for damage detection (Aloisio et al. 2020, 2021; Viefhues et al. 2022).

### ***Bridge Damage Detection using the Influence Lines (ILs)-based Method***

By contrast, relatively rare attention has been paid to static damage detection approaches, such as dead-load redistribution change and IL-based indices. Although ILs are often related to moving loads in the literature, ILs are essentially structural static characteristics. IL-based indices inherit the advantages and essence of moving load-based approaches, and further show their merits as easy removal of the zero drift and the variation caused by temperature load. Zaurin and Catbas (2009) proposed to identify the strain IL (SIL) of a four-span bridge model by combining video imaging and sensing information, and they subsequently testified that SIL was a promising damage indicator through a four-span bridge-type structure and a steel bascule bridge (Zaurin and Catbas 2011; Zaurin et al. 2016). Chen et al. (2015) proposed three stress IL-based damage localization indicators for long-span bridges. The effectiveness of these indicators was validated through the numerical case studies of the full-scale TMB. Later, Zhu et al. (2014) integrated the stress IL-based indices with the data fusion method to enhance the detectability. Subsequently, they verified these IL-based damage localization indices and the improved approach experimentally on a three-span concrete beam model (Chen et al. 2017). To realize damage quantification, Chen et al. (2018) reconstructed the deflection IL (DIL) using the matrix decomposition method, and revealed the relationship between structural damage and DIL change in beam structures. The effectiveness of the quantification method was experimentally validated through a simply supported beam. Cai et al. (2022) have recently compared different IL-based indices, revealed their intrinsic relationships, and shed light on selecting appropriate IL-based indices and optimizing sensor placement on beam structures. Huseynov et al. (2020) adopted the rotation IL (RIL) change before and after damage as a damage index. They realized damage localization experimentally in a simply supported beam model. A similar RIL-based index was also used by Alamdari et al. (2019a), who verified this index numerically in a cable-stayed bridge. Other studies on IL-based damage detection in the last decade are summarized in Table 1. Meanwhile, many identification methods, which identified ILs from moving vehicle-induced dynamic responses of a bridge, were proposed and proved numerically or experimentally (Chen et al. 2015; 2016; Wang et al. 2017; Frøseth et al. 2017; Dong et al. 2019; Zheng et al. 2020).

Notably, ILs are typical bridge characteristics that are frequently measured in trial tests before the bridge opening and regular load testing during the service life of bridges by using heavy trucks. With bridge health monitoring systems, ILs can be measured or identified in a more convenient and timely manner. ILs have also been applied to bridge capacity evaluation (Wang et al. 2022a), weight-in-motion (Lansdell et al. 2017), and model updating (Zhu et al. 2015). However, the corresponding discussions are not included in the scope of the current

study.

### ***Research Objectives***

Previous studies have demonstrated the prospect of the vibration- and IL-based damage indices. Most of these indices were tested on simple structural configurations with a limited number of unknown parameters, such as simply supported beams; thus, they lack practicality for real bridge applications to some extent. Detecting local damages in a large-scale complex bridge remains a major challenge. Moreover, investigations on IL-based methods for long-span bridges are rare, although ILs were proven superior to dynamic characteristics (e.g., modal properties) in some aspects of damage detection. Two relevant studies are the numerical case studies on the TMB (Chen et al. 2015; Zhu et al. 2014) and the condition assessment on the Yangtze Bridge (Sun et al. 2016). Although bridge ILs are regularly measured, creating man-made damages in real bridges and investigating the detectability of these IL-based indices are certainly impractical. Therefore, experimental investigation on ILs for damage detection in long-span bridges is of practical significance.

The present study experimentally investigates the IL-based damage localization method in a long-span bridge by using a scaled physical model of the TMB as an example. The main contributions of this experimental work are as follows: (1) The effectiveness of the IL-based damage indices for long-span bridges was experimentally validated for the first time. (2) The damage detection performances of the IL-based and the modal properties-based methods in long-span bridges are experimentally compared. After the Introduction, Section 2 elaborates on why IL can be employed for damage detection and recalls the IL-based damage localization methods, including IL change and its first-order finite difference, in previous numerical studies. Then, Section 3 introduces the scaled physical model of the TMB used for the subsequent experimental investigation. Section 4 presents the experimental performance of the IL-based indices on the TMB model. Both single- and double-damage scenarios are considered. Section 5 presents the detection performance of the modal properties-based methods. Finally, the major findings and conclusions are summarized in Section 6.

## **ILs for Damage Detection**

### ***Mechanics of ILs for Damage Detection***

Structural damage detection is typically defined as detecting the stiffness reduction of one or more structural members. The inverse of the stiffness matrix is the flexibility matrix, which has been used for model updating and damage identification because of its superiority in damage sensitivity. In conventional vibration-based approaches, the flexibility matrix is constructed from the modal properties (Zonta et al. 2003):

$$\mathbf{F} = \mathbf{\Phi}\mathbf{\Omega}^{-1}\mathbf{\Phi}^T, \quad (1)$$

where  $\mathbf{F}$  is the flexibility matrix,  $\mathbf{\Phi}$  is the mode shape matrix, and  $\mathbf{\Omega}$  is the diagonal matrix containing modal frequencies. However, the flexibility matrices constructed from modal properties have limited accuracy and practicability because of the following: (1) obtaining mass-normalized mode shapes is usually difficult; (2) dynamic signals are vulnerable to measurement noise; (3) mode truncations are usually performed, as the number of measurable vibration modes is usually much lower than the number of the degree of freedom (DOF); and (4) flexibility has a low spatial resolution if only a limited number of sensors are used (Zonta et al. 2003; Chen et al. 2015).

The DIL describing the deflection response variation at a specific location when a unit force moves along a beam (or a bridge) is essentially part of the flexibility matrix (Chen et al. 2018). The moving force acts sequentially on a series of selected vertical DOFs; in this scene, the load matrix for obtaining ILs can be represented as follows:

$$\mathbf{Q} = \begin{bmatrix} 1 & 0 & 0 & \cdots & \cdots & 0 & 0 & \cdots & \cdots & 0 \\ & 1 & & \vdots \\ & & \ddots & \vdots \\ & & & 1 & 0 & \cdots & \cdots & 0 & 0 & \cdots & \cdots & 0 \end{bmatrix}^T, \quad (2)$$

where  $\mathbf{Q}$  is the load matrix. The identity submatrix on the left side of Eq. (2) corresponds to the vertical DOFs with a unit force, while the remaining zero submatrix corresponds to the vertical, horizontal, and rotational DOFs without any force. Given the relationship between flexibility matrix, load matrix, and deflection matrix,

$$\mathbf{D} = \mathbf{F}\mathbf{Q}, \quad (3)$$

where  $\mathbf{D}$  is the DIL matrix. The DIL measured at the  $i$ th DOF is essentially part of the  $i$ th row of the flexibility matrix. Accordingly, multiple DILs at several DOFs can represent a submatrix of the flexibility matrix. Therefore, DILs can reflect the flexibility matrix to some extent. Similar mechanics are also applicable to RILs and SILs. Moreover, various ILs represent static structural characteristics, which are quite different from dynamic characteristics. Notably, estimating the complete flexibility matrix of a long-span bridge based on the limited IL measurement information is impossible because the practical moving force direction is only vertical.

Similarly, the SIL can be represented by multiplying load matrix  $\mathbf{Q}$  and strain flexibility matrix  $\mathbf{F}^e$ :

$$\mathbf{D}^e = \mathbf{F}^e\mathbf{Q}, \quad (4)$$

where  $\mathbf{D}^e$  is the SIL matrix. The strain flexibility matrix was also referred to as the damage index by Zonta et al. (2003).

### ***IL-based Damage Indices***

As mentioned in the literature review, changes in different types of ILs and their derivatives were investigated for damage detection, and their effectiveness was partially validated in some structural configurations (Chen et al. 2015; 2018; Huseynov et al. 2020).

The basic type is the IL change representing the direct change in flexibility,

$$\Delta \mathbf{IL}(x, y) = \mathbf{IL}(x, y) - \mathbf{IL}_b(x, y), \quad (5)$$

where  $\mathbf{IL}(x, y)$  and  $\mathbf{IL}_b(x, y)$  are the newly obtained IL function and the IL function in the healthy (undamaged) state, respectively;  $x$  is the force location in the bridge (beam) longitudinal direction; and  $y$  is the sensor location. Once the bridge suffers from severe local damage, the measured IL change exhibits distinct features at damage locations, typically either a peak or a sudden drop. The shapes of the damage-induced IL changes for different IL types were analytically and experimentally compared by Cai et al. (2022) by using a simply supported beam as an illustrated example.

The first-order finite difference of the IL change is also explored as a damage index to enhance the damage sensitivity:

$$\Gamma(x, y) = \Delta \mathbf{IL}(x + \Delta x, y) - \Delta \mathbf{IL}(x, y), \quad (6)$$

where  $\Delta x$  is the spatial interval between two force steps. Although the high-order finite difference of IL change can further enhance damage sensitivity, it may simultaneously amplify the noise effect, causing false alarms. Deflection and strain typically represent the global and local responses, respectively; both DIL and SIL were investigated in the present study.

### **Scaled TMB Model**

The TMB is one of the longest suspension bridges in the world. It carries a highway and a railway. A comprehensive structural health monitoring system has been installed on this bridge since 1997, including 110 strain gauges (Wong et al. 2000). A corresponding physical scaled bridge model, wherein all the major connections and boundary conditions were reproduced with a geometric scale of 1:150, was established at The Hong Kong Polytechnic University (Xu et al. 2012; 2016).

Fig. 1 shows the schematic of the scaled TMB model. Its total length and main span are 14.34 and 9.18 m, respectively, and the height of the two towers is 1.37 m. Two main cables are 0.24 m apart in the lateral direction. Same as the real TMB, the scaled TMB model displays the deck suspended at the main span and the west side span (Ma Wan side), while the deck is

supported by three supports in the east side span (Tsing Yi side). The dimension of this scaled model is large enough to allow the installation of various sensors for response monitoring. Two different materials were used for fabricating this scaled bridge model: aluminum was used for the bridge deck, whereas steel was used for other components, such as bridge towers, piers, cables, and suspenders. Fig. 1(b) shows a typical cross frame. The whole bridge model consists of 242 cross frames connected by two outer and two inner longitudinal trusses by welding. In this study, one cross frame and its nearby right longitudinal trusses were defined as one module (Mod.); thus, this bridge model has 241 modules plus an additional cross frame. The length of each module is around 6 mm in the bridge longitudinal direction. Fig. 1(c) shows two typical modules between the two suspenders of this model, mainly comprising the top chord, bottom chord, diagonal chord, vertical post, railway beam, and bottom beam. Xu et al. (2012) presented the specific design and fabrication of this scaled model. A corresponding finite element model (FEM) was established, and model updating was conducted based on the measured modal characteristics of the scaled model. Since then, a few structural health monitoring studies have been conducted on this scaled TMB testbed. Xu et al. (2016) developed a multitype sensor optimal placement and response reconstruction method and validated the effectiveness through this scaled TMB model. Xu et al. (2018) employed this TMB model for experimental validation of a multilevel damage detection method with response reconstruction using a divide-and-conquer approach. Notably, the IL-based method in the present study is a model-free method, and it used only the measurement information from the physical model and did not need the FEM.

## **Experimental Validation**

### ***Experimental Setup***

Fig. 2 shows the schematic of the experimental setup. Displacement sensors and strain gauges were installed at the selected locations of the model to obtain the corresponding IL information. A total of 46 strain gauges (model no. BX120-3AA) and four displacement sensors (model no. KEYENCE, LK-503) were deployed on the TMB model. Given the symmetrical cross frame of the deck, all strain gauge sensors were placed on the left side (i.e., Grid I and II in Fig. 3) in this study. The strain and displacement response information was collected by two data acquisition systems (model no. KYOWA EDX-100A) with a sampling frequency of 10 Hz for the IL measurement in the static tests. Moreover, 19 additional accelerometers (model no. KD1010 and KD1300) were installed on the main span bridge deck to obtain the modal information. The sampling frequency was changed to 1000 Hz during the acceleration measurement in the dynamic test.

The spatial installation configuration of these sensors is shown in Fig. 3. The zoom-in

blocks, representing the specific regions instrumented with strain gauges, show the specific spatial installation layout. The bridge topology is complex and consists of several components with different individual element properties (e.g., stiffness). Thus, the strain gauge installation covered as many components as possible in one selected region (i.e., the bottom-right block in Fig. 3). This region was selected because the preliminary FEM analysis indicated relatively large strain amplitudes of the structural components in this region. Detailed information on sensor installation is presented in Table 2. A steel block of 5.5 kg representing a moving mass was placed on the aluminum bridge deck of every other module during static IL measurement, where no dynamic amplification effect needs to be considered. However, if IL is obtained from the dynamic responses induced by a vehicle with a high running speed, the dynamic amplification factor has to be carefully dealt with. Fig. 4 shows the corresponding photograph of the setup of the scaled TMB model.

### *Characteristics of ILs*

Fig. 5 shows the characteristics of the SILs measured at different bridge components in one module (i.e., Mod. 114), wherein the abscissa is the force location and the ordinate is the variation of the SIL coefficient. The profiles of these SILs were markedly different: (1) The SIL curves of the top and bottom chords were approximately opposite. (2) The SIL curves of the railway beam and bottom chord were nearly symmetric with respect to the sensor location, whereas the SIL curve of the diagonal chord was nearly antisymmetric. (3) A sharp peak appeared in the SIL curves of the vertical post and bottom beam. The profile characteristics of the measured SIL curves were similar to those observed in the full-scale TMB FEM (Chen et al. 2015). Moreover, the strain influence coefficient decreased when the force moved away from the sensor location. According to Chen et al. (2015), the peak-to-peak amplitude, defined as the difference between the maximum and minimum strain, and the boundary of the main coverage range, defined as the 30% of the amplitude, were determined to quantify the characteristics of different SILs, as summarized in Table 3. The SIL amplitudes of the longitudinal components, i.e., the bottom and top chords and railway beam, were relatively greater than others. The SIL amplitudes of the vertical post and bottom beam attenuated quickly with the increasing distance, both exhibiting a narrow coverage range. Although the SIL of the diagonal chord exhibited the largest coverage range, it might not be suitable for damage detection because of the smallest peak strain magnitude. Based on the above observations, the SILs of the railway beam and the bottom and top chords were selected to detect local damages in such a long-span bridge.

Fig. 6 shows a typical DIL of the bridge deck varying with the force location. The maximum deflection coefficient in this scene was approximately 9 mm, which corresponded to nearly 1.35 m in the full-scale bridge. The DIL curve was approximately symmetric about the

sensor location. Similar to SIL, DIL was characterized by an amplitude of 11.5 mm and a coverage range of 56 modules. The coverage range of DILs was wider than that of SILs, indicating that DIL is a global detection index, whereas SIL is a relatively local one.

### ***Damage Detection Performance***

Given that the TMB is a statically indeterminate structure, any damage would result in the internal loading redistribution. Accordingly, the ILs, regardless of DILs or SILs, extracted from the undamaged components near the damaged members would also exhibit differences. Considering the components with relatively larger strain/stress amplitudes are more vulnerable to train- or vehicle-induced fatigue damage, the bottom chords member was selected as the damaged members in this study. The present study simulated two damage scenarios in the bottom chords, as seen in Fig. 7. Both were produced in Grid I, close to the strain gauge installation layout.

- The first damage scenario was made by cutting the bottom chord of Mod. 112, referred to as a single-damage case.
- The second damage scenario was simulated by cutting another bottom chord of Mod. 100, referred to as a double-damage case.

The bottom chords of the bridge are subjected to tension under a vertical external load. The two damaged bottom chords were selected at the locations that were associated with relatively large tensile stress in the preliminary FEM analysis and thus considered vulnerable to fatigue damage.

### ***Single-damage Case***

Fig. 8 shows the representative results of the ILs before and after damage, wherein the SIL was measured from the bottom chord of Mod. 109, and the DIL was measured from the bridge deck of Mod. 114. The two vertical lines denote the sensor and damage locations. Although the SIL and DIL curves showed peaks at the sensor location, both the SIL and DIL change curves exhibited obvious peak values corresponding to the damage locations. Both the SIL and DIL change curves were almost symmetric with respect to the damage location. In this study, the change ratio of the IL is defined as the ratio between the peak-to-peak amplitude of IL change and the corresponding IL. The SIL and DIL change ratios were approximately 40% and 3.4%, respectively, demonstrating that SIL is more sensitive to local damage than DIL. The slight change ratio of DIL (i.e., 3.4%) indicated that a single structural truss component loss in such a complex long-span bridge has a limited effect on the overall structural performance, highlighting the difficulties in damage detection in complex long-span bridges using global indices directly. Consequently, only SIL results were used for damage localization in the

following sections unless otherwise stated.

Fig. 9 shows the SIL change ratio of different bridge components near the damaged bottom chord, which is shown by a dashed line. The lines with different lightness (or colors) were used to represent different change levels of SILs, namely, <10%, 10%–20%, 20%–30%, 30%–40%, and >40%. In particular, Fig. 10 presents the IL change of different bridge components of Mod. 114. An apparent peak indicating the damage location could be observed at all the concerned bridge components, despite the disturbance caused by the measurement noise. The SIL change of the bottom beam exhibited another sharp peak due to the sensing problem when the mass acted near the strain gauge. In descending order of the damage-induced strain change amplitude, the top three components were the bottom chord, railway beam, and top chord; these components exhibited dozens of microstrains change. As shown in Figs. 9 and 10, the bottom chord damage was relatively easy to be detected by the bottom chord and railway beam by considering the IL change amplitude and change ratio jointly.

In addition, the SIL changes extracted from different railway beams and bottom chords were investigated, as shown in Fig. 11. The corresponding change ratio is presented in Fig. 12. The SIL change of the railway beam and bottom chord generally decreased with the increasing distance between the sensors and damage location. The SIL change ratio of the bottom chord was generally larger than that of the railway beam, given the same distance. For the bottom chords and railway beams, the SILs of Mods. 107 and 120 could still identify the damage at Mod. 112 accurately, whereas those SILs of Mods. 95 and 133 could not. This finding demonstrated that the detectable range of SIL was approximately 10 modules ( $\approx 0.6$  m), corresponding to approximately 4% of the whole length of the TMB model. Therefore, installing strain gauges on the longitudinal horizontal components every 10 modules could guarantee satisfactory detection performance in the entire bridge model.

Fig. 13 shows the damage detection results using the mentioned first-order finite difference of the IL change by taking the SIL of the bottom chord of Mod. 109 and the DIL of Mod. 114 as examples. Although the calculation of finite difference amplified the noise effect, the damage location could still be located by identifying the sudden change of either SIL or DIL. This result demonstrated the effectiveness of the first-order finite difference-based indices for damage detection in long-span bridges and confirmed the findings of the previous numerical study using a full-scale FEM (Chen et al. 2015).

#### *Double-damage Case*

As mentioned, the second damage was done by cutting off the bottom chord of Mod. 100. Fig. 14 shows the corresponding detection results using the SIL change of the bottom chords in Mods. 95 and 107. Only one apparent peak corresponding to the damage location could be

identified visually in each SIL result. The peak locations were different: the SIL result extracted from Mod. 95 located the damage at Mod. 100, whereas that from Mod 107 located the damage at Mod. 112. Notably, according to Fig. 11, the detectable range of SIL in the single-damage case was approximately 10 modules. However, the SIL change of Mod. 107 cannot locate the second damage at Mod. 100 in this double-damage case. The reason is that the SIL of Mod. 107 was more sensitive to the damage in Mod. 112 due to the closer distance, whereas the corresponding SIL change of Mod. 107 induced by the Mod. 100 damage was much smaller and cannot be clearly identified. Note that the SIL change ratio of Mod. 107 was approximately 26% in the single-damage case (as shown in Fig. 12), whereas it only slightly increased to 28.5% because of the introduced second damage. These results implied the limited detectable range of the SILs again. Multiple SIL information will be required for multidamage detection in long-span bridges.

## **Comparison with Modal Parameters**

In the dynamic test, the accelerometers were also deployed on the bridge's main span, and a hammer was used to generate an impact signal. The corresponding modal information, including modal frequencies and mode shapes, was extracted by using the complex mode indicator function (Brincker et al. 2001) based on the measured accelerations. The change in modal frequencies and mode shapes were regarded as the vibration-based damage indices to identify the damage (single-damage case). Only the vertical vibration modes were considered in this study.

Fig. 15 depicts the extracted first three mode shape information of the main span of the bridge model before and after the single-damage simulation. The difference was quite small; the damage occurrence could not be identified based on this difference. The first vertical mode shape was almost antisymmetric, whereas the second vertical mode was symmetric with a half-wave, regardless of whether the damage occurred or not. The modal assurance criterion (MAC) (Pastor et al. 2012) was applied to detect damage occurrence. Table 4 lists the specific vertical modal frequencies information and the calculated MAC values. The maximum natural frequency change was merely 2.6%, and the MAC values were above 0.99. The change ratios of the modal information in Table 4 were much smaller than that in Fig. 9 (mostly > 10%). The limited number of sensors led to the low spatial resolution of the mode shapes. As a result, the modal curvatures could not be accurately computed, and the corresponding detection performance was poor. The experimental results indicated that compared with the SIL-based indices, the modal parameter change might not be suitable for the direct detection of the local damages in long-span bridges. It was also noted that the identified natural frequencies were slightly different from those reported by Xu et al. (2012) due to the recent change in the TMB

model.

## Conclusions

In this study, damage detection in a long-span bridge using ILs was experimentally investigated for the first time through a scaled model. The scaled TMB testbed at The Hong Kong Polytechnic University was used as a representative long-span bridge example. Different types of sensors, including displacement sensors, strain gauges, and accelerometers, were deployed in this model. First, the DIL characteristics of the bridge deck and the SIL characteristics of different bridge components of the TMB model, including bottom chords, top chords, railway beams, bottom beams, vertical posts, and diagonal chords, were investigated. Subsequently, both single- and double-damage cases were simulated at the bottom chords of different modules. The IL extracted from a single sensor can effectively locate the single damage; multiple IL information is required for the double-damage case. The damage detection performance in the physical scaled TMB model demonstrated that SIL is a good local damage index for long-span bridges, which will shed light on structural health monitoring in real-world full-scale bridges. The following specific damage detection results are remarked:

- 1) In the single-damage scenario, the damage-induced change ratio of the SIL was much larger than that of the DIL. This finding demonstrated that SILs might be more suitable for local damage detection than DILs, performing higher damage detectability.
- 2) Although all the SILs of the nearby bridge components could identify damage occurrence and location, the damage in the bottom chord tended to be detected by the bottom chords and railway beams more easily by considering the SIL change amplitudes and ratios together.
- 3) The SIL change ratio decreased with the increasing distance between the sensor and the damage locations. The detectable range of SILs was limited but with a relatively high damage sensitivity near the damage location.
- 4) The first-order finite difference of the IL change successfully identified the single-damage location without any noise elimination process, even though the finite difference calculation amplified the noise effect.
- 5) In the case study, the direct utilization of the SIL change (i.e., Eq. (5)) extracted from a single sensor could not locate double damages because of the limited damage range and relatively large distance between the installed sensor and damage locations. Thus, multiple sensor applications should be required.
- 6) Corresponding to the first three vertical vibration modes, the single local damage-induced maximum frequency change ratio was less than 3%, and all the MAC values were higher

than 0.99. This finding indicated that compared with the IL-based indices, the straightforward usage of the modal parameters might not be a suitable approach for damage detection in long-span bridges.

Considering the limited detectable range of SILs, a sufficient number of strain measurements will be required to cover the range of the entire long-span bridge. Distributed strain measurement, a recently-emerging sensing technology that provides strain information with high spatial resolution, will be a promising solution to be used jointly with the IL-based damage detection method investigated in this study. In addition, because of the destructive nature of the presented experiments, only two damage scenarios could be tested in this paper. More comprehensive investigations of various damage scenarios will be done through numerical simulations. All of these need to be addressed in future studies.

## Data Availability Statement

All the presented data that support the findings of this study are available from the corresponding author upon reasonable request.

## Acknowledgments

The authors are grateful for the financial support provided by the National Key R&D Program of China (2019YFB1600700), the National Natural Science Foundation of China (NSFC-52278319), the GDSTC Key Technologies R&D Program (2019B111106001), the Research Grants Council of Hong Kong (T22-502/18-R, PolyU 15214620), and The Hong Kong Polytechnic University (BBWJ, ZE2L, ZVX6). The first author also gratefully acknowledges the support from the Postdoc Matching Fund Scheme provided by The Hong Kong Polytechnic University (W21P). All authors thank Prof. You-Lin Xu for providing the opportunity to conduct the experiments on the TMB testbed. The findings and opinions expressed in this paper are from the authors alone and do not necessarily represent the views of the sponsors.

## References

- Alamdari, M. M., Kildashti, K., Samali, B., and Goudarzi, H. V. (2019a). "Damage diagnosis in bridge structures using rotation influence line: Validation on a cable-stayed bridge." *Eng. Struct.*, 185, 1-14. <https://doi.org/10.1016/j.engstruct.2019.01.124>.
- Alamdari, M. M., Ge, L., Kildashti, K., Zhou, Y., Harvey, B., and Du, Z. (2019b). "Non-contact structural health monitoring of a cable-stayed bridge: Case study." *Struct. Infrastruct. Eng.*, 15(8), 1119-1136. <https://doi.org/10.1080/15732479.2019.1609529>.
- Aloisio, A., Di Battista, L., Alaggio, R., and Fragiaco, M. (2020). "Sensitivity analysis of

- subspace-based damage indicators under changes in ambient excitation covariance, severity and location of damage.” *Eng. Struct.*, 208, 110235. <https://doi.org/10.1016/j.engstruct.2020.110235>.
- Aloisio, A., Alaggio, R., and Fragiaco, M. (2021). “Bending stiffness identification of simply supported girders using an instrumented vehicle: full scale tests, sensitivity analysis, and discussion.” *J. Bridge Eng.*, 26(1), 04020115. [https://doi.org/10.1061/\(ASCE\)BE.1943-5592.0001654](https://doi.org/10.1061/(ASCE)BE.1943-5592.0001654).
- Breccolotti, M., and Natalicchi, M. (2022). “Bridge damage detection through combined quasi-static influence lines and weigh-in-motion devices. *Int. J. Civ. Eng.*, 20(5), 487-500. <https://doi.org/10.1007/s40999-021-00682-0>.
- Brincker, R., Zhang, L., and Andersen, P. (2001). “Modal identification of output-only systems using frequency domain decomposition.” *Smart Mater. Struct.*, 10(3), 441. <https://doi.org/10.1088/0964-1726/10/3/303>.
- Briseghella, B., Fa, G., Aloisio, A., Pasca, D., He, L., Fenu, L., and Gentile, C. (2021). “Dynamic characteristics of a curved steel–concrete composite cable-stayed bridge and effects of different design choices.” *Structures*, 34, 4669-4681. <https://doi.org/10.1016/j.istruc.2021.10.060>.
- Cai, Q., Chen, Z., Zhu, S., and Mo, L. (2022). “On damage detection of beam structures using multiple types of influence lines.” *Structures*, 42, 449-465. <https://doi.org/10.1016/j.istruc.2022.06.022>.
- Cawley, P., and Adams, R. D. (1979). “The location of defects in structures from measurements of natural frequencies.” *J. Strain Anal. Eng. Des.*, 14(2), 49-57. <https://doi.org/10.1243/03093247V142049>.
- Chen, Z. W., Zhu, S., Xu, Y. L., Li, Q., and Cai, Q. L. (2015). “Damage detection in long suspension bridges using stress influence lines.” *J. Bridge Eng.*, 20(3), 05014013. [https://doi.org/10.1061/\(ASCE\)BE.1943-5592.0000681](https://doi.org/10.1061/(ASCE)BE.1943-5592.0000681).
- Chen, Z. W., Cai, Q. L., and Li, J. (2016). “Stress influence line identification of long suspension bridges installed with structural health monitoring systems.” *Int. J. Struct. Stab. Dyn.*, 16(04), 1640023. <https://doi.org/10.1142/S021945541640023X>.
- Chen, Z. W., Yang, W., Jun, L., Cheng, Q., and Cai, Q. L. (2017). “A systematic method from influence line identification to damage detection: Application to RC bridges.” *Comput. Concr.*, 20(5), 563-572. <https://doi.org/10.12989/cac.2017.20.5.563>.
- Chen, Z. W., Cai, Q. L., and Zhu, S. (2018). “Damage quantification of beam structures using deflection influence lines.” *Struct. Contr. Health Monit.*, 25(11), e2242.

<https://doi.org/10.1002/stc.2242>.

- Dong, C.-Z., Bas, S., and Catbas, F. N. (2019). “A completely non-contact recognition system for bridge unit influence line using portable cameras and computer vision.” *Smart Struct. Syst.*, 24(5), 617-630. <https://doi.org/10.12989/sss.2019.24.5.617>.
- Frøseth, G. T., Rønnquist, A., Cantero, D., and Øiseth, O. (2017). “Influence line extraction by deconvolution in the frequency domain.” *Comput. Struct.*, 189, 21-30. <https://doi.org/10.1016/j.compstruc.2017.04.014>.
- Huseynov, F., Kim, C., O'Brien, E. J., Brownjohn, J., Hester, D., and Chang, K. (2020). “Bridge damage detection using rotation measurements—Experimental validation.” *Mech. Syst. Signal Pr.*, 135, 106380. <https://doi.org/10.1016/j.ymsp.2019.106380>.
- He, W. Y., and Zhu, S. (2016). “Moving load-induced response of damaged beam and its application in damage localization.” *J. Vib. Control*, 22(16), 3601-3617. <https://doi.org/10.1177/1077546314564587>.
- He, W. Y., Ren, W. X., and Zhu, S. (2017). “Damage detection of beam structures using quasi-static moving load induced displacement response.” *Eng. Struct.*, 145, 70-82. <https://doi.org/10.1016/j.engstruct.2017.05.009>.
- Jang, S., Jo, H., Cho, S., Mechitov, K., Rice, J. A., Sim, S.-H., Jung, H.-J., Yun, C.-B., Spencer Jr, B. F., and Agha, G. (2010). “Structural health monitoring of a cable-stayed bridge using smart sensor technology: deployment and evaluation.” *Smart Struct. Syst.*, 6(5-6), 439-459. [https://doi.org/10.12989/sss.2010.6.5\\_6.439](https://doi.org/10.12989/sss.2010.6.5_6.439)
- Lansdell, A., Song, W., and Dixon, B. (2017). “Development and testing of a bridge weigh-in-motion method considering nonconstant vehicle speed.” *Eng. Struct.*, 152, 709-726. <https://doi.org/10.1016/j.engstruct.2017.09.044>.
- Li, J., and Zhao, X. (2006). “A super-element approach for structural identification in time domain.” *Front. Math. Eng. China*, 1(2), 215-221. <https://doi.org/10.1007/s11465-006-0004-4>.
- Link, M., and Weiland, M. (2009). “Damage identification by multi-model updating in the modal and in the time domain.” *Mech. Syst. Signal Pr.*, 23(6), 1734-1746. <https://doi.org/10.1016/j.ymsp.2008.11.009>.
- Liu, X., Lieven, N., and Escamilla-Ambrosio, P. J. (2009). “Frequency response function shape-based methods for structural damage localisation.” *Mech. Syst. Signal Pr.*, 23(4), 1243-1259. <https://doi.org/10.1016/j.ymsp.2008.10.002>.
- Liu, Y., and Zhang, S. (2018). “Damage localization of beam bridges using quasi-static strain influence lines based on the BOTDA technique.” *Sensors*, 18(12), 4446.

<https://doi.org/10.3390/s18124446>.

- Lu, Z., and Law, S. (2007). “Features of dynamic response sensitivity and its application in damage detection.” *J. Sound Vib.*, 303(1-2), 305-329. <https://doi.org/10.1016/j.jsv.2007.01.021>.
- Ni, Y., Zhou, H., Chan, K., and Ko, J. (2008). “Modal flexibility analysis of cable - stayed Ting Kau Bridge for damage identification.” *Comput-Aided Civ. Inf.*, 23(3), 223-236. <https://doi.org/10.1111/j.1467-8667.2008.00521.x>
- Pandey, A., Biswas, M., and Samman, M. (1991). “Damage detection from changes in curvature mode shapes.” *J. Sound Vib.*, 145(2), 321-332. [https://doi.org/10.1016/0022-460X\(91\)90595-B](https://doi.org/10.1016/0022-460X(91)90595-B).
- Pastor, M., Binda, M., and Harčarik, T. (2012). “Modal assurance criterion.” *Procedia Eng.*, 48, 543-548. <https://doi.org/10.1016/j.proeng.2012.09.551>.
- Ren, J., Zhang, B., Zhu, X., and Li, S. (2022). “Damaged cable identification in cable-stayed bridge from bridge deck strain measurements using support vector machine.” *Adv. Struct. Eng.*, 25(4), 754-771. <https://doi.org/10.1177/13694332211049996>.
- Sharry, T., Guan, H., Nguyen, A., Oh, E., and Hoang, N. (2022). “Latest advances in finite element modelling and model updating of cable-stayed bridges.” *Infrastructures*, 7(1), 8. <https://doi.org/10.3390/infrastructures7010008>.
- Sun, S., Sun, L., and Chen, L. (2016). “Damage detection based on structural responses induced by traffic load: Methodology and application.” *Int. J. Struct. Stab. Dyn.*, 16(04), 1640026. <https://doi.org/10.1142/S0219455416400265>.
- Viefhues, E., Döhler, M., Hille, F., and Mevel, L. (2022). “Statistical subspace-based damage detection with estimated reference.” *Mech. Syst. Signal Pr.*, 164, 108241. <https://doi.org/10.1016/j.ymssp.2021.108241>.
- Wang, N. B., He, L.-X., Ren, W. X., and Huang, T. L. (2017). “Extraction of influence line through a fitting method from bridge dynamic response induced by a passing vehicle.” *Eng. Struct.*, 151, 648-664. <https://doi.org/10.1016/j.engstruct.2017.06.067>.
- Wang, N. B., Ren, W. X., and Huang, T. L. (2019). “Baseline-free damage detection method for beam structures based on an actual influence line.” *Smart Struct. Syst.*, 24(4), 475-490. <https://doi.org/10.12989/sss.2019.24.4.475>
- Wang, N. B., Zuo, Q., Li, J., and Huang, T. L. (2021). “Damage detection method for statically indeterminate bridge based on multi-influence line information in current state.” *J. of Cent. South Univ.*, 52(9), 3284-3294 (In Chinese). <https://10.11817/j.issn.1672-7207.2021.09.030>

- Wang, N. B., Shen, W., Guo, C., and Wan, H. P. (2022a). "Moving load test-based rapid bridge capacity evaluation through actual influence line." *Eng. Struct.*, 252, 113630. <https://doi.org/10.1016/j.engstruct.2021.113630>.
- Wang, X., Wang, L., Wang, H., Ning, Y., Huang, K., and Wang, W. (2022b). "Performance evaluation of a long-span cable-stayed bridge using non-destructive field loading tests." *Appl. Sci.*, 12(5), 2367. <https://doi.org/10.3390/app12052367>.
- Wickramasinghe, W. R., Thambiratnam, D. P., Chan, T. H., and Nguyen, T. (2016). "Vibration characteristics and damage detection in a suspension bridge." *J. Sound Vib.*, 375, 254-274. <https://doi.org/10.1016/j.jsv.2016.04.025>
- Wong, K. Y., Lau, C., and Flint, A. (2000) "Planning and implementation of the structural health monitoring system for cable-supported bridges in Hong Kong." *Proc., Nondestructive evaluation of highways, utilities, and pipelines IV, SPIE*, 266-275. <https://doi.org/10.1117/12.387819>
- Xu, Y. L., Zhang, X., Zhan, S., Hong, X., Zhu, L., Xia, Y., and Zhu, S. (2012). "Testbed for structural health monitoring of long-span suspension bridges." *J. Bridge Eng.*, 17(6), 896-906. [https://doi.org/10.1061/\(ASCE\)BE.1943-5592.0000349](https://doi.org/10.1061/(ASCE)BE.1943-5592.0000349).
- Xu, Y. L., Zhang, X. H., Zhu, S., and Zhan, S. (2016). "Multi-type sensor placement and response reconstruction for structural health monitoring of long-span suspension bridges." *Sci. Bull.*, 61(4), 313-329. <https://doi.org/10.1007/s11434-016-1000-7>.
- Xu, Y. L., Zhang, C. D., Zhan, S., and Spencer, B. F. (2018). "Multi-level damage identification of a bridge structure: A combined numerical and experimental investigation." *Eng. Struct.*, 156, 53-67. <https://doi.org/10.1016/j.engstruct.2017.11.014>.
- Xu, Z. D., and Wu, Z. (2007). "Energy damage detection strategy based on acceleration responses for long-span bridge structures." *Eng. Struct.*, 29(4), 609-617. <https://doi.org/10.1016/j.engstruct.2006.06.004>.
- Xu, Z. D., Liu, M., Wu, Z., and Zeng, X. (2011). "Energy damage detection strategy based on strain responses for long-span bridge structures." *J. Bridge Eng.*, 16(5), 644-652. [https://doi.org/10.1061/\(ASCE\)BE.1943-5592.0000195](https://doi.org/10.1061/(ASCE)BE.1943-5592.0000195).
- Zaurin, R., and Catbas, F. (2009). "Integration of computer imaging and sensor data for structural health monitoring of bridges." *Smart Mater. Struct.*, 19(1), 015019. <https://doi.org/10.1088/0964-1726/19/1/015019>.
- Zaurin, R., and Necati Catbas, F. (2011). "Structural health monitoring using video stream, influence lines, and statistical analysis." *Struct. Health Monit.*, 10(3), 309-332. <https://doi.org/10.1177/1475921710373290>.

- Zaurin, R., Khuc, T., and Catbas, F. N. (2016). "Hybrid sensor-camera monitoring for damage detection: case study of a real bridge." *J. Bridge Eng.*, 21(6), 05016002. [https://doi.org/10.1061/\(asce\)be.1943-5592.0000811](https://doi.org/10.1061/(asce)be.1943-5592.0000811).
- Zeinali, Y., and Story, B. A. (2018). "Impairment localization and quantification using noisy static deformation influence lines and Iterative Multi-parameter Tikhonov Regularization." *Mech. Syst. Signal Pr.*, 109, 399-419. <https://doi.org/10.1016/j.ymssp.2018.02.036>
- Zhang, Y. M., Wang, H., Bai, Y., Mao, J. X., and Xu, Y. C. (2022). "Bayesian dynamic regression for reconstructing missing data in structural health monitoring." *Struct. Health Monit.*, 21(5), 2097-2215. <https://doi.org/10.1177/14759217211053779>
- Zheng, X., Yang, D. H., Yi, T. H., and Li, H. N. (2020). "Bridge influence line identification from structural dynamic responses induced by a high-speed vehicle." *Struct. Contr. Health Monit.*, 27(7), e2544. <https://doi.org/10.1002/stc.2544>.
- Zheng, X., Yi, T. H., Yang, D.-H., and Li, H. N. (2021). "Stiffness estimation of girder bridges using influence lines identified from vehicle-induced structural responses." *J. Eng. Mech.*, 147(8), 04021042. [https://doi.org/10.1061/\(asce\)em.1943-7889.0001942](https://doi.org/10.1061/(asce)em.1943-7889.0001942)
- Zhu, Q., Xu, Y. L., and Xiao, X. (2015). "Multiscale modeling and model updating of a cable-stayed bridge. I: Modeling and influence line analysis." *J. Bridge Eng.*, 20(10), 04014112. [https://doi.org/10.1061/\(asce\)be.1943-5592.0000722](https://doi.org/10.1061/(asce)be.1943-5592.0000722).
- Zhu, S., Chen, Z., Cai, Q., Lei, Y., and Chen, B. (2014). "Locate damage in long-span bridges based on stress influence lines and information fusion technique." *Adv. Struct. Eng.*, 17(8), 1089-1102. <https://doi.org/10.1260/1369-4332.17.8.1089>.
- Zhou, Y., Di, S., Xiang, C., Li, W., and Wang, L. (2018) "Damage identification in simply supported bridge based on rotational-angle influence lines method." *Trans. Tianjin Univ.*, 24(6), 587-601. <https://doi.org/10.1007/s12209-018-0135-9>.
- Zonta, D., Lanaro, A., and Zanon, P. (2003) "A strain-flexibility-based approach to damage location." *Proc., Key Eng. Mater., Trans. Tech. Publ.*, 87-96. <https://doi.org/10.4028/www.scientific.net/KEM.245-246.87>.

## **Table Caption List**

Table 1 IL-based indices reported in previous studies

Table 2 Sensor installation in the TMB model

Table 3 Characteristics of the measured SILs from different bridge components: Mod. 114

Table 4 Modal-information-based indicator for damage detection

## Tables

Table 1 IL-based indices reported in previous studies

IL type	Model	Study type	References
SIL	Four-span bridge-type structure	Experiment	Zaurin and Catbas 2011
SIL	Bascule bridge	Field test	Zaurin et al. 2016
Stress IL	TMB (suspension bridge)	Numerical	Chen et al. 2015
Stress IL	TMB (suspension bridge)	Numerical	Zhu et al. 2014
DIL, SIL	Three-span concrete beam	Experiment	Chen et al. 2017
DIL	Simply supported beam	Experiment	Chen et al. 2018
DIL, RIL, SIL	Simply supported beam	Experiment	Cai et al. 2022
RIL	Simply supported beam	Experiment	Huseynov et al. 2020
RIL	Simply supported truss bridge	Numerical	Zhou et al. 2018
SIL	Shanghai Yangtze River Bridge (Cable-stayed bridge)	Field test	Sun et al. 2016
RIL	Cable-stayed bridge	Numerical	Alamdari et al. 2019a
DIL	Cable-stayed bridge	Numerical	Alamdari et al. 2019b
DIL	Simply supported beam	Experiment	Zeinali and Srory 2018
DIL	Simply supported beam	Experiment	Wang et al. 2019
DIL, SIL	Three-span beam	Numerical	Wang et al. 2021
DIL, RIL	Three-span beam	Numerical	Zheng et al. 2021
SIL	Simply supported bridge	Experiment	Liu and Zhng 2018
DIL, RIL	Simply supported bridge; Multi-span continuous bridge	Numerical	Breccolotti and Natalicchi 2022

Table 2 Sensor installation in the TMB model

Sensor type	Bridge Component	Mod. No. (Locations)
Strain gauge	Railway beam	95, 107, 109, 111, 113–115, 117, 118, 120, 122, 133, 173
	Top chord	95, 113–115, 118, 133, 173
	Bottom chord	95, 107, 109, 111, 113–115, 117, 118, 120, 122, 133, 173
	Diagonal chord	95, 113–115, 133, 173
	Bottom beam	113–115
	Vertical post	113–115
Laser displacement sensor	Bridge deck	95, 114, 133, 173
Accelerometer	Bridge deck	60, 68, 76, 84, 92, 100, 108, 116, 124, 132, 140, 148, 156, 164, 172, 180, 188, 196, 204

Table 3 Characteristics of the measured SILs from different bridge components: Mod. 114

Component	Maximum ( $\mu\epsilon$ )	Minimum ( $\mu\epsilon$ )	Amplitude ( $\mu\epsilon$ )	Coverage range (no. of modules.)
Railway beam	126.4	-37.2	163.6	24
Top chord	45.4	-123.5	168.9	21
Bottom chord	98.0	-20.1	118.1	18
Diagonal chord	6.7	-4.8	11.5	62
Vertical post	12.2	-4.0	16.2	1
Bottom beam	28.6	-6.2	34.8	2

Table 4 Modal-information-based indicator for damage detection

Mode number	Frequency (Hz)		Change ratio	MAC
	Undamaged	Damage		
First order	5.30	5.16	2.6%	0.9987
Second order	5.62	5.49	2.4%	0.9993
Third order	9.66	9.64	0.2%	0.9991

## Figure Caption Lists

- Fig. 1 Configuration of the TMB model: (a) Overview of the TMB model; (b) Cross-frame model; (c) Bridge components of two typical modules
- Fig. 2 Schematic of the experimental setup for the TMB model
- Fig. 3 Spatial configuration of the applied sensors in the TMB model (numbers “1” to “240” denote the Mod. number)
- Fig. 4 Photograph of the experimental setup
- Fig. 5 SILs of different bridge components: (a) Component locations; (b) Set A; (c) Set B; (d) Set C
- Fig. 6 DIL of bridge deck: Mod. 114
- Fig. 7 Photograph of damage locations (DL is short for damage location): (a) DL1; (b) DL2
- Fig. 8 ILs before and after single damage: (a) SIL of bottom chord: Mod. 109; (b) DIL of bridge deck: Mod. 114
- Fig. 9 SIL change ratios for different bridge components near the damage
- Fig. 10 SIL change of different bridge components: Mod. 114: (a) Railway beam; (b) Bottom beam; (c) Bottom chord; (d) Top chord; (e) Vertical post; (f) Diagonal chord
- Fig. 11 SIL change of bottom chord and railway beam: (a) Bottom chord; (b) Railway beam
- Fig. 12 Change ratios of SILs with sensor locations
- Fig. 13 Damage localization results using the first-order finite difference of IL change: (a) SIL of bottom chord: Mod. 109; (b) DIL of bridge deck: Mod. 114
- Fig. 14 Damage localization results for double-damage case: (a) Mod. 95; (b) Mod. 107
- Fig. 15 Identified mode shapes before and after single-damage simulation: (a) First order; (b) Second order; (c) Third order

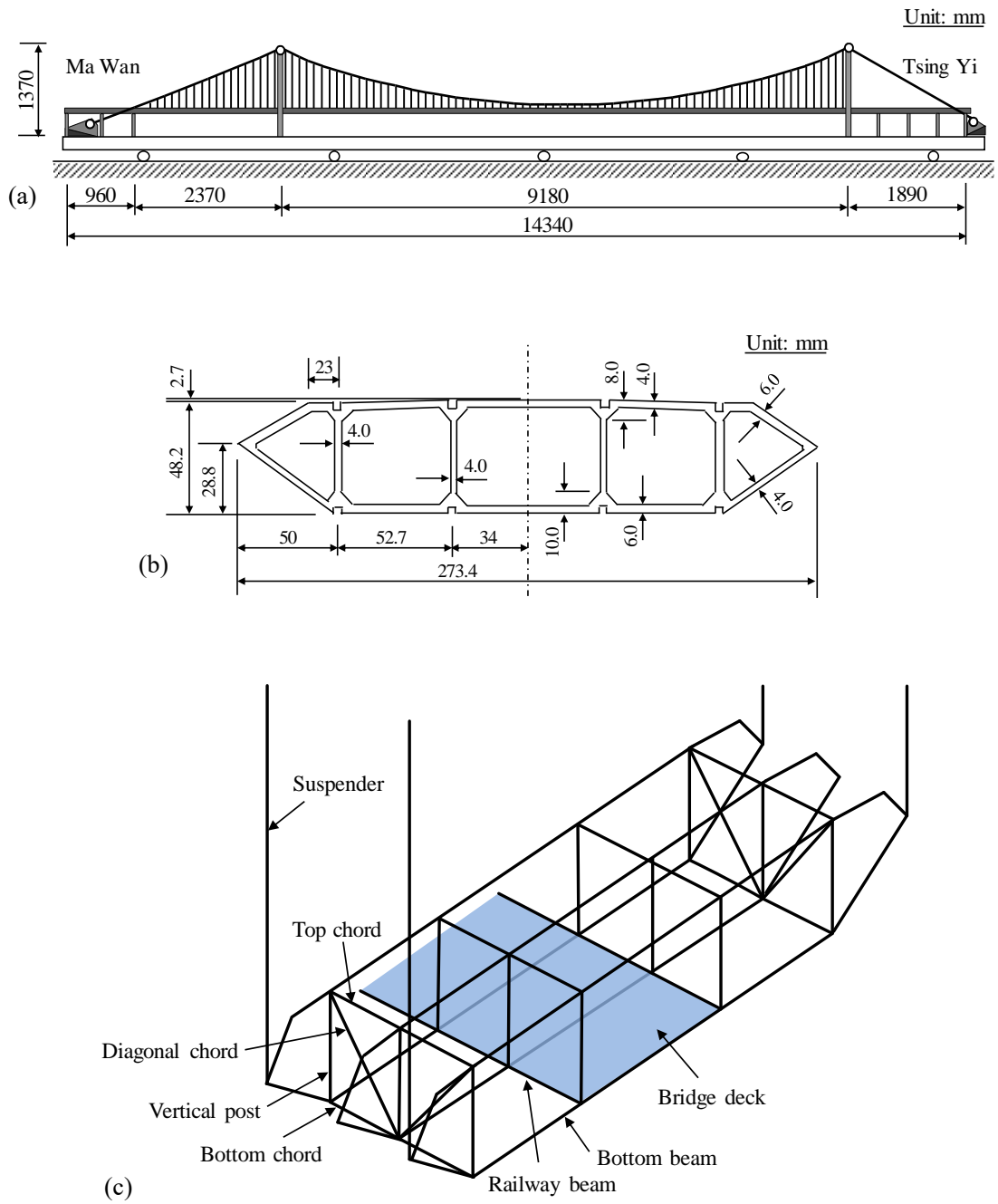


Fig. 1 Configuration of the TMB model: (a) Overview of the TMB model; (b) Cross-frame model; (c) Bridge components of two typical modules

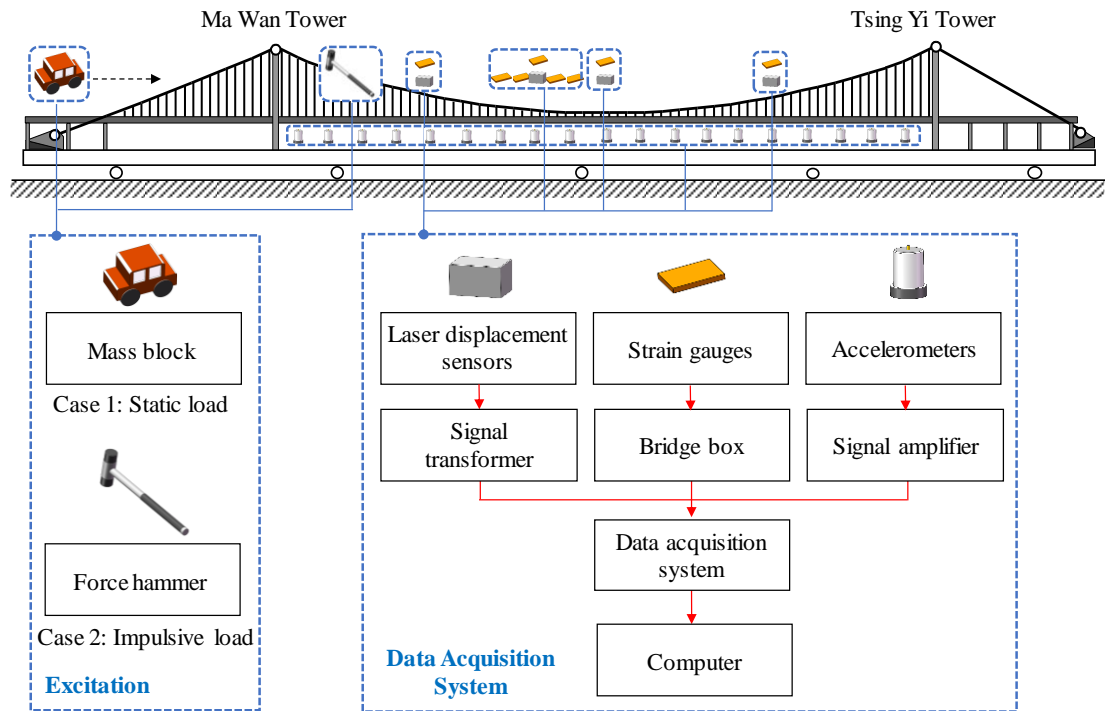


Fig. 2 Schematic of the experimental setup for the TMB model

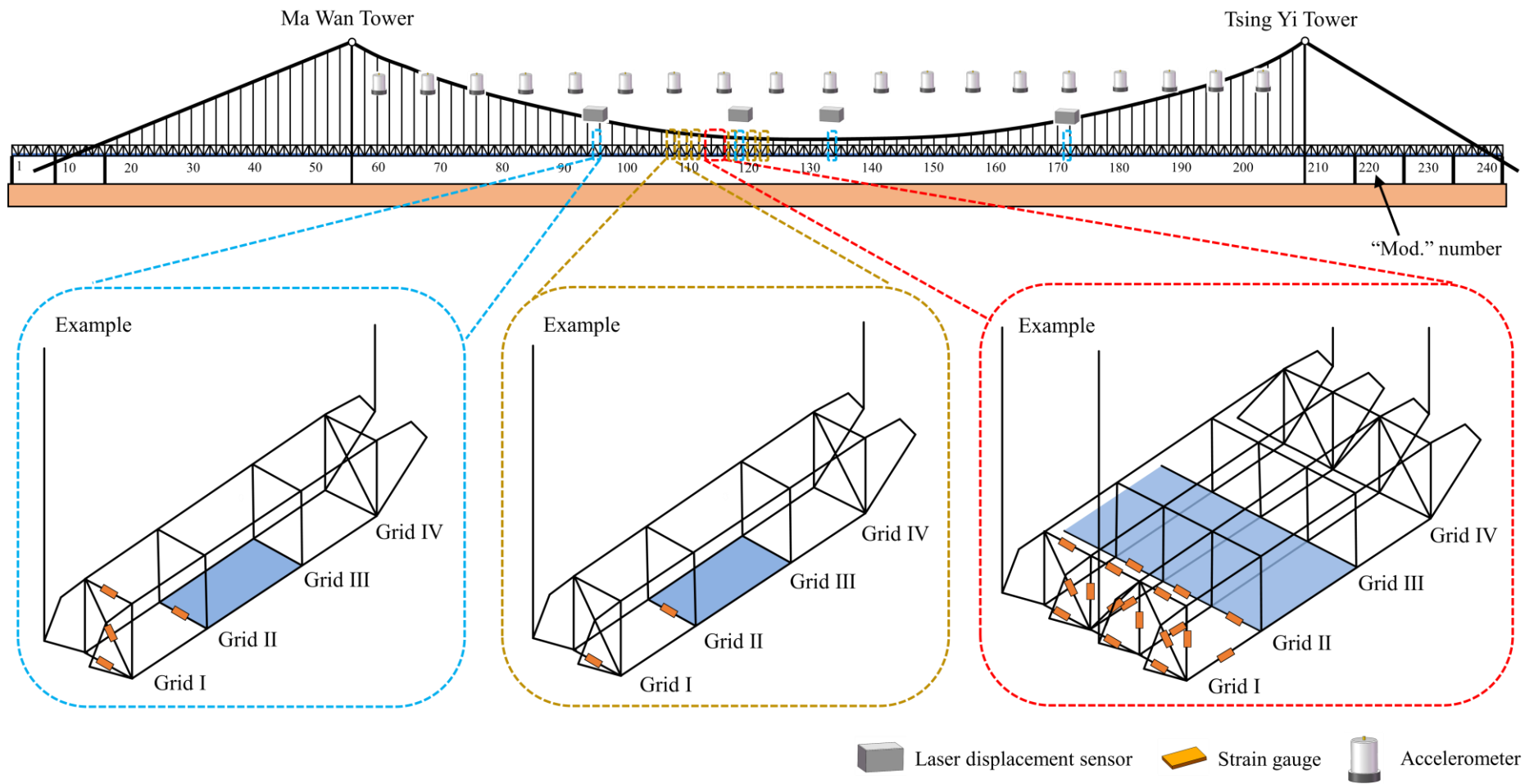


Fig. 3 Spatial configuration of the applied sensors in the TMB model (numbers “1” to “240” denote the Mod. number)



Fig. 4 Photograph of the experimental setup

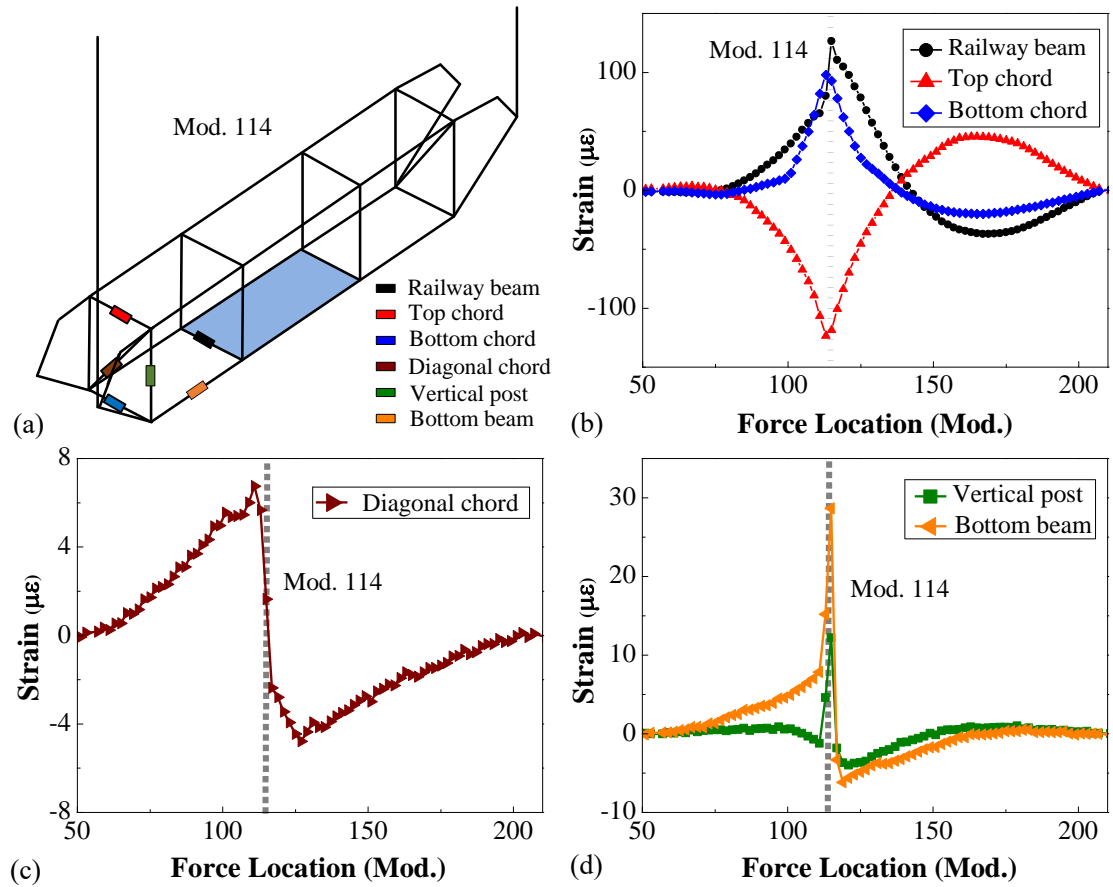


Fig. 5 SILs of different bridge components: (a) Component locations; (b) Set A; (c) Set B; (d) Set C

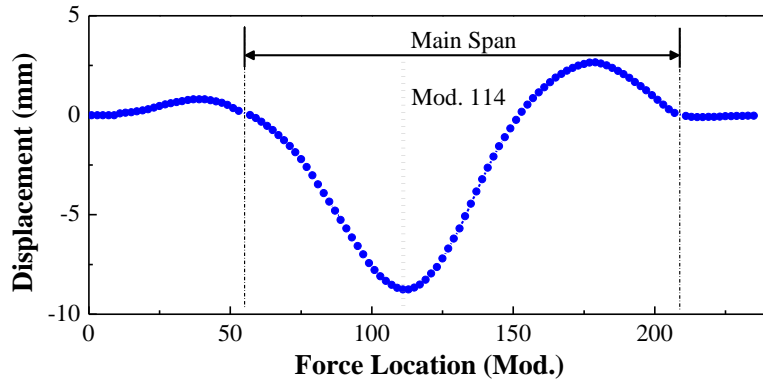


Fig. 6 DIL of bridge deck: Mod. 114

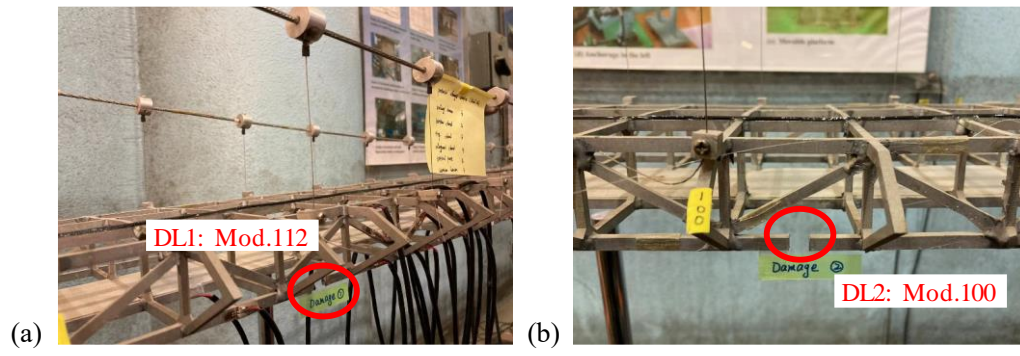


Fig. 7 Photograph of damage locations (DL is short for damage location): (a) DL1; (b) DL2

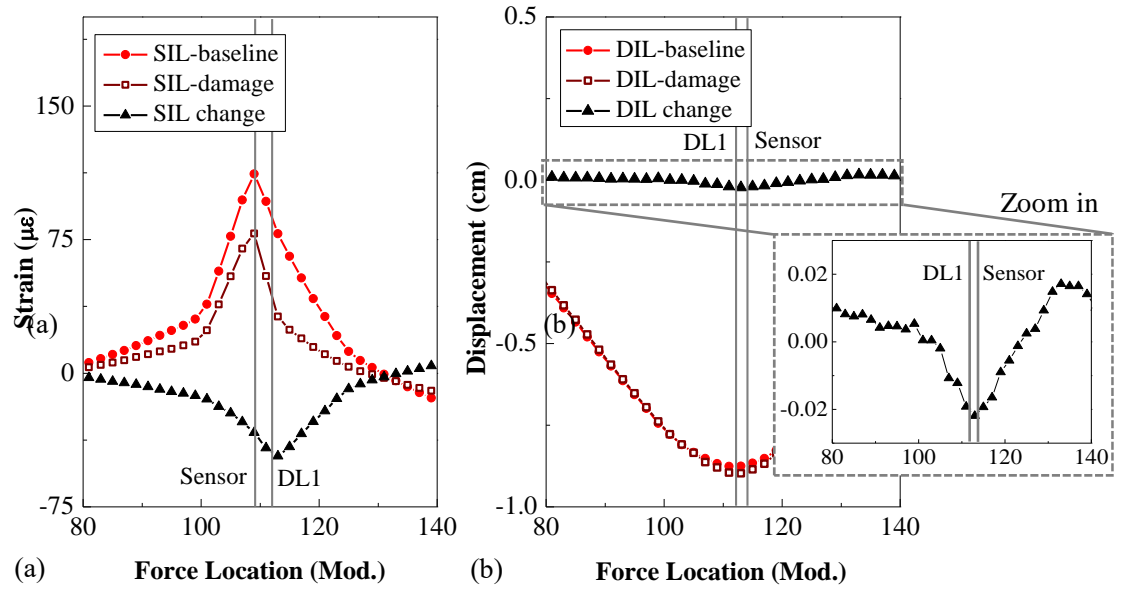


Fig. 8 ILs before and after single damage: (a) SIL of bottom chord: Mod. 109; (b) DIL of bridge deck: Mod. 114

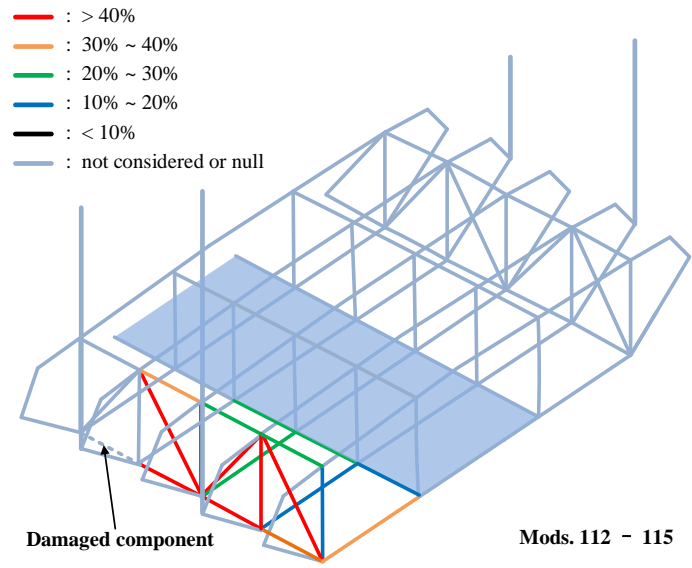


Fig. 9 SIL change ratios for different bridge components near the damage

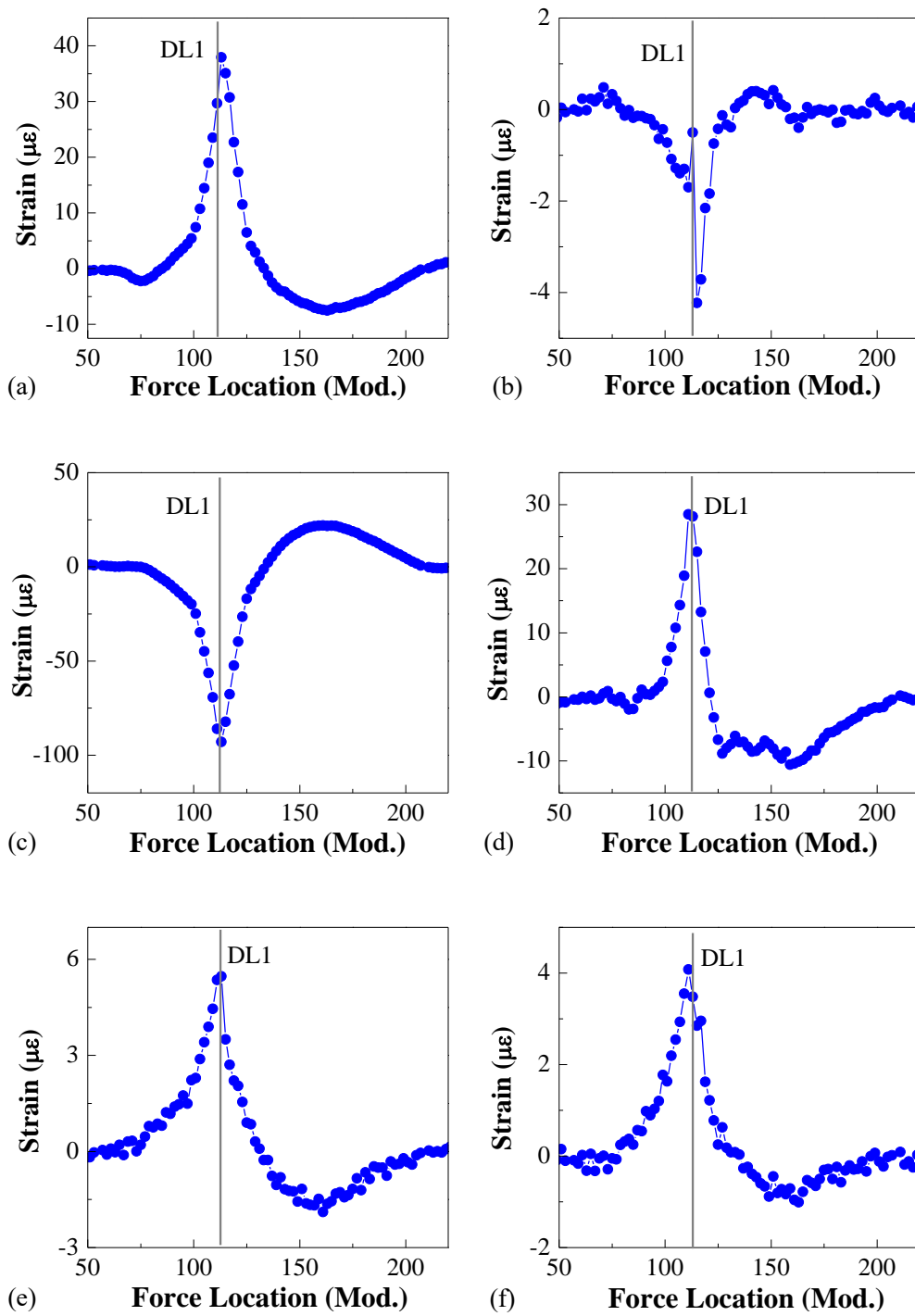


Fig. 10 SIL change of different bridge components: Mod. 114: (a) Railway beam; (b) Bottom beam; (c) Bottom chord; (d) Top chord; (e) Vertical post; (f) Diagonal chord

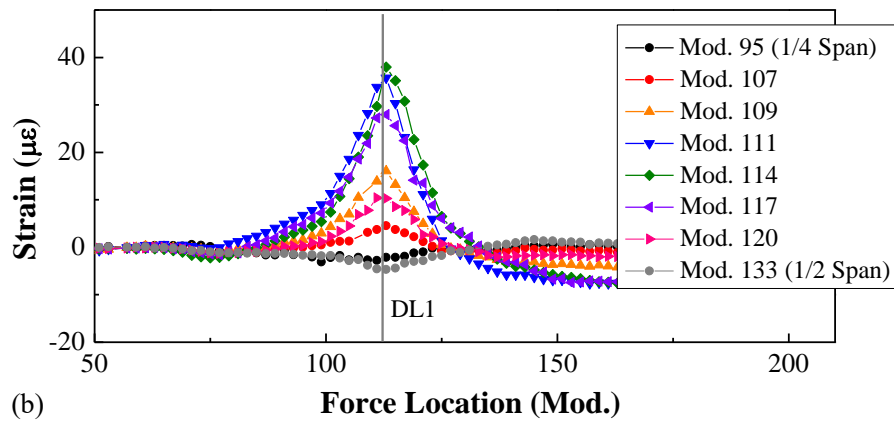
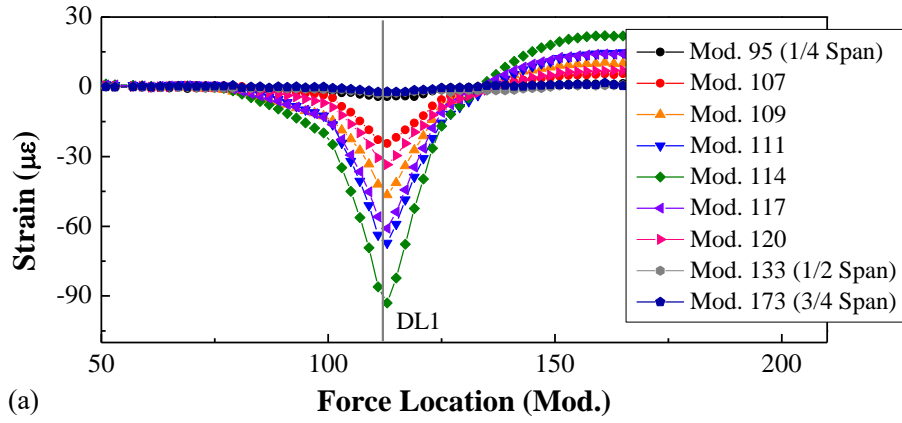


Fig. 11 SIL change of bottom chord and railway beam: (a) Bottom chord; (b) Railway beam

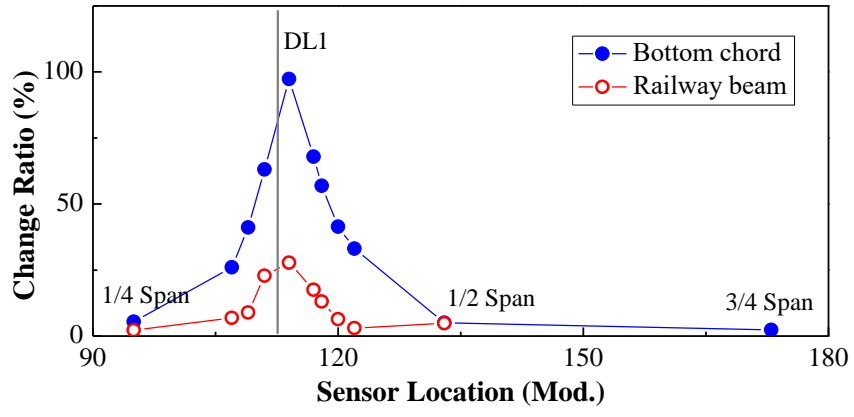


Fig. 12 Change ratios of SILs with sensor locations

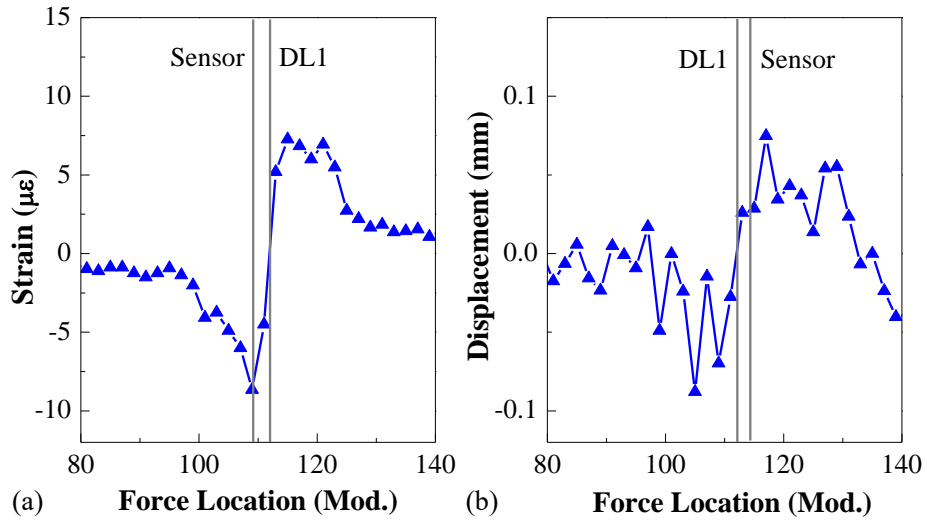


Fig. 13 Damage localization results using the first-order finite difference of IL change: (a) SIL of bottom chord: Mod. 109; (b) DIL of bridge deck: Mod. 114

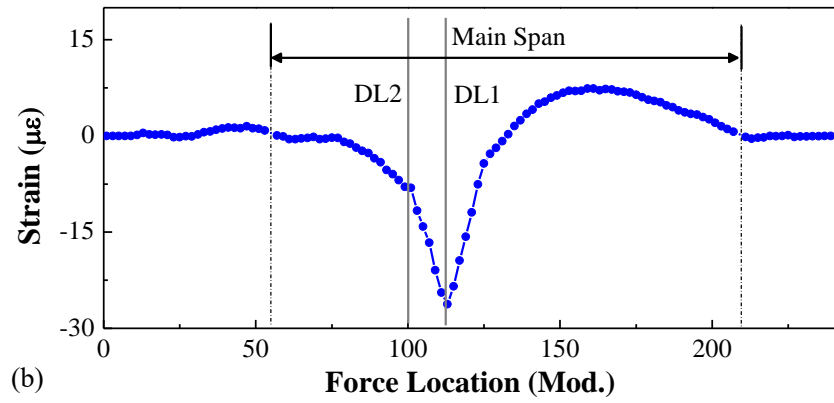
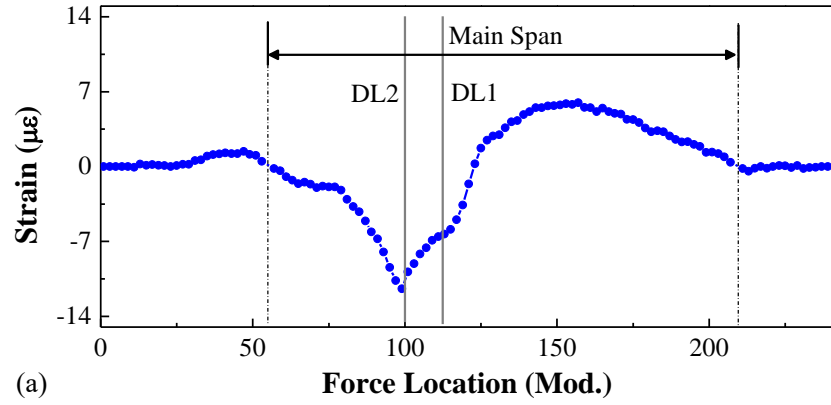


Fig. 14 Damage localization results for double-damage case: (a) Mod. 95; (b) Mod. 107

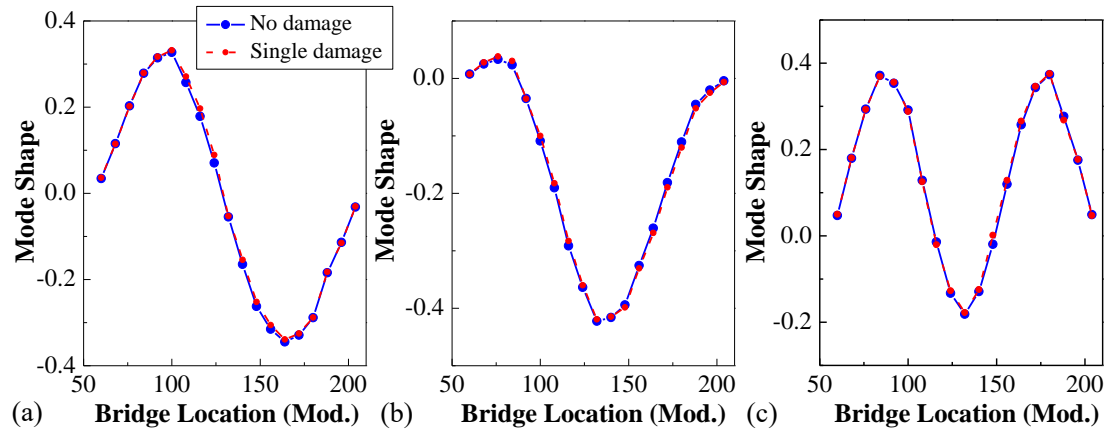


Fig. 15 Identified mode shapes before and after single-damage simulation: (a) First order; (b) Second order; (c) Third order